Journal of the European Ceramic Society 20 (2000) 997–1002

Indium-containing ceramics with negative temperature coefficient characteristics

C. Metzmacher*, R. Mikkenie, W.A. Groen

Philips Research Laboratories, PO Box 500145, D-52085 Aachen, Germany

Received 10 March 1999; received in revised form 13 July 1999; accepted 8 August 1999

Abstract

Different phases of the transition metal oxide system of indium–manganese–nickel have been studied by means of X-ray diffraction. The electrical properties of the spinel phases have been characterized by measurement of the specific resistivity and activation energy indicating a negative temperature coefficient (NTC) material. The replacement of Mn by In in the system Ni–Mn–O results in the formation of single phase spinels with higher specific resistivities and thermal constant values. In three series with fixed Ni amounts of 0.30, 0.45 and 0.60 the cubic-to-tetragonal phase transition takes place at nearly the same In content of 0.78. Secondary phases like In_2O_3 and NiO have been found in samples with a Ni content of 0.60 if the total In concentration exceeds 1.32. A linear increase of the thermal constant and logarithmic resistivity for samples with a nickel content of 0.45 and 0.60 as a function of the indium content have been observed.

Keywords: Electrical properties; Phase analysis; Spinels; Thermistors; Transition metal oxides; NTC

1. Introduction

Negative temperature coefficient ceramics (NTC) or thermistors are semiconducting ceramics consisting of transition metal oxides. Their resistivity, ρ, varies exponentially with temperature T by the well known Arrhenius equation $\rho = \rho_0 \exp(B/T)$ which expresses the concept of a thermally sensitive resistor. Here, ρ_0 is the resistivity of the material at infinite temperature and B is the thermal constant which is related to the activation energy E_a for electrical conduction according to $B = E_a/k$ (k: Boltzmann's constant). Typically, the resistance R of these thermistors lies in the range of 10 to $10^5\Omega$, and B is 2000–5000 K. These ceramics are widely used in temperature measurement and control. It is believed that the conductivity is due to a thermally activated phonon-assisted hopping mechanism of charge carriers between cations of differing oxidation state on crystallographically equivalent lattice sites. As a consequence the mobility of the charge carriers is very low and is described as small polarons.

There is a large choice of NTC materials, but those most used in practice are based on solid solutions of oxides with the spinel structure of general formula $A[B_2]O_4$. In this structure a cubic close packed array of oxygen ions allows two types of lattice sites available for the cations with tetrahedral (often stated as "A-site") and octahedral ("B-site", indicated by [...]) symmetry, respectively. As there is a extensive variety for the A and B ions and a strong dependence on production conditions (sintering temperature, atmosphere and cooling rate), the lattice site occupation can change between the two extremes of a so-called normal spinel $A[B_2]O_4$ and an inverse one $B[AB]O_4$.

A series that gives favourable combinations of low resistivity and high coefficients of B comprises the naturally insulating $Mn_3O_4 = Mn^{2+}[Mn_2^{3+}]O_4^{2-}$ with partial replacement of Mn by Ni, Co, Cu, Fe.[1–3] This substitution produces Mn^{4+} ions and therefore pairs of Mn^{3+} and Mn^{4+} on the octahedral sites, e.g. $NiMn_2O_4 = Ni_{1-\delta}^{2+}Mn_{\delta}^{2+}[Ni_{\delta}^{2+}Mn_{2-2\delta}^{3+}Mn_{\delta}^{4+}]O_4^{2-}$, where it is assumed to find some of the nickel on tetrahedral sites, too, which indicates a so-called inversion degree δ. This leads to semiconducting properties and conduction by electron or hole transfer. Additionally, the localized distortion induced by Mn^{3+} in an octahedral crystal

* Corresponding author. Tel.: +49-241-6003-427; fax: +49-241-6003-465.

E-mail address: christof.metzmacher@philips.com (C. Metzmacher).

0955-2219/00/$ - see front matter
PII: S0955-2219(99)00207-1

field can result in the cooperative Jahn-Teller effect which leads to a tetragonal crystal structure.

In the system Ni–Mn–O materials can be prepared which exhibit a good long term stability of the resistivity and the B value. However, only a specific set of so-called R_{25} merits (resistance measured at a temperature $T=25°C$) and $B_{25/85}$ (comparison with R value at $T=85°C$) values can be prepared in this system. In order to achieve higher $B_{25/85}$ values some Fe is added to this system which leads to an increase of R_{25}, too. The problem which arises in these compounds is the long-term stability of the resistance, i.e. the aging phenomena. In Refs. 4 and 5, the addition of Li to the Ni–Mn–O spinel system is stated to result in a more thermodynamic stable system with high stability of the resistance. Similar claims are made for the addition of Mg[6] and Zn[7] to the system Ni–Mn–O and Ba to the system Ni–Cu–Mn–O.[8]

The starting point of our considerations is the desire to increase the range of practical useful R and B values in a new system of NTC materials. The present investigations indicate that the addition of In to the system Ni–Mn–O results in the formation of single phase spinel compounds with higher specific resistivities and $B_{25/85}$ values. With respect to the fact that the aging problem with the iron doped samples might be related to the different oxidation states that exist for Fe (2+, 3+), to the complex distribution of the iron ions over the different crystallographic sites in the spinel[9] and to the corresponding migration between tetrahedral and octahedral lattice sites,[3] the advantage of the use of In over Fe might be that for In only one oxidation state (3+) exists under these conditions, thus a thermodynamically more stable system could probably be expected.

2. Experimental

In this work the phase diagram of Mn–Ni–In–O was analysed in order to investigate how much indium can be substituted in the Ni–Mn–oxide spinels. All samples were processed by solid state reaction starting from the oxides Mn_2O_3, NiO and In_2O_3, respectively. Stoichiometric mixtures of the metal oxides were prepared yielding to $Mn_{2.33-z}In_zNi_{0.67}O_4$ with $z=0$, 1/12, 1/6, 1/3 and 2/3, to the boundary systems Ni–Mn, In–Mn and Ni–In, respectively, and additionally to samples with fixed Ni content y of 0.60, 0.45 and 0.30 in the oxide system of $Mn_{3-y-x}In_xNi_yO_4$ with different x between 0 and 1.5 as given in the following section. After milling and homogenization in isopropylalcohol with ceramic balls overnight followed by drying, pellets were pressed from the mixed powders and sintered for 16 h at 1300°C in air. All samples were quenched to room temperature simply by cooling in air in order to try to avoid oxidation and to retain the high-temperature characteristic properties. Phase analysis and microstructural investigations of the sinterskin free pellets were performed using X-ray diffraction (XRD) on a Philips PW1080 diffractometer (U = 40 kV, I = 35 mA) with APD 1700 software, secondary monochromator and proportional counter. The experimental parameters were a wavelength of $\lambda=1.5418$ Å (Cu-K_α radiation), a step scan of 0.15°/min and a divergence slit of 1°. The errors in lattice calculation can be estimated to be less than 0.005 and 0.01 Å in the case of a cubic and tetragonal spinel structure, respectively. Electrical contacts on the pellets were made by vacuum deposition and the resistance and thermal constant values (for both error $<0.2\%$) were determined with the aid of a self-built equipment which contains of a thermostat bath with silicone oil and a multimeter controlled by a PC. Scanning electron microscopy (SEM) was performed for secondary electron imaging on a Philips XL30 FEG at an operating voltage of 20 kV.

3. Results and discussion

3.1. Indium doped NTC ceramics

The unit cell parameters calculated from the diffraction data as a function of the indium content for the composition $Mn_{2.33-z}In_zNi_{0.67}O_4$ are presented in Fig. 1. This plot shows an increase of the lattice constant if manganese is substituted by indium. Furthermore, Vegard's law is obeyed indicating that all indium is incorporated in the spinel lattice. The results concerning the R_{25} and $B_{25/85}$ values are presented in Fig. 2. Both, the specific resistivity and the energy values increase with increasing indium content in $Mn_{2.33-z}In_zNi_{0.67}O_4$. This series shows that materials with interesting properties can be achieved and therefore we decided to look for the boundary phase systems in order to clarify in which region a single spinel phase can be produced.

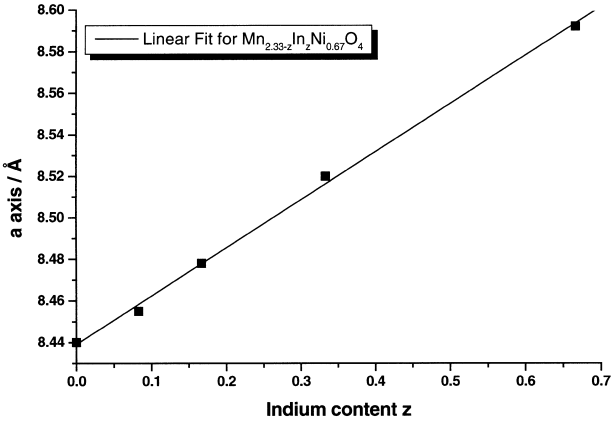

Fig. 1. The unit cell parameter a calculated from X-ray diffraction data as a function of the indium content z in $Mn_{2.33-z}In_zNi_{0.67}O_4$.

3.2. The phase system Mn–Ni–In–O

Ni–Mn compositions were made according to the formula $Ni_uMn_{3-u}O_4$ with $u=0$, 0.25, 0.46, 0.54 and 0.60. For increasing u there is a single spinel phase with decreasing tetragonal distortion up to $u=0.55$. This is due to the fact that the addition of Ni^{2+} on the octahedral sites lowers the concentration of the Mn^{3+} ions on these sites, causing a decreasing cooperative Jahn-Teller effect and smaller lattice distortion. If u is larger than 0.55 NiO appears as a second phase besides the tetragonal spinel. This is an agreement with the results presented by Larson et al.[10] An increase in temperature leads to a decomposition of the spinel into NiO and a Mn-rich tetragonal spinel.

In–Mn compositions with the formula $In_{2-v}Mn_vO_3$ ($v_{max}=0.25$) were prepared. The lattice constant of the cubic bixbyite structure of In_2O_3 decreases linearly with increasing Mn according to Vegard's law up to $v=0.14$ ($a=10.078$ Å). For higher v values a compound similiar to the tetragonal hausmannite structure is found additionally. Mn-rich samples were also investigated according to the composition $In_wMn_{3-w}O_4$ ($w_{max}=0.54$). Up to $w=0.3$ indium oxide can be dissolved into the manganese oxide spinel with a slight decrease of the tetragonal distortion with increasing w. If w is higher than 0.3, the cubic bixbyite structure appears as a second phase. Finally, in the system Ni–In no ternary phases have been found.

In Fig. 3 a first order approximation of the oxide phase diagram of Mn–Ni–In is given which was determined with additional compositions as stated in the previous section. The single phase cubic and tetragonal spinel ranges denoted "C" and "T" in Fig. 3, respectively, are of special interest and are presented in more detail below. The fields which extend from "C" and "T" to the corner points of Ni and In correspond to multiphase areas and have not been characterized in greater extent here.

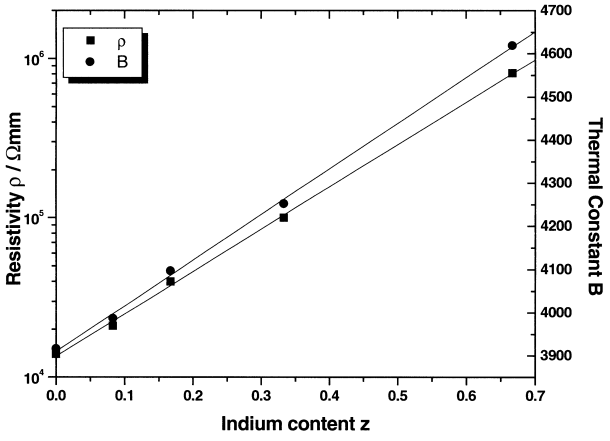

Fig. 2. The specific resistivity ρ and the thermal constant $B_{25/85}$ as a function of the indium content z in $Mn_{2.33-z}In_zNi_{0.67}O_4$ (linear fit for eye guidance only).

3.3. Single phase compounds

Three series with fixed Ni content y have been analyzed, i.e. the compounds $Ni_{0.60}Mn_{2.40-x}In_xO_4$, $Ni_{0.45}Mn_{2.55-x}In_xO_4$ and $Ni_{0.30}Mn_{2.70-x}In_xO_4$. The lattice constants a and c which are calculated from XRD experiments are given in Fig. 4 as a function of In content x. The unit cell was chosen to be a pseudo-cubic face-centred cell with $c>a$ to be comparable to the cubic spinel structure. The density of the sintered ceramic pellets has been determined by Archimedis principle to be better than 98% of the theoretical value.

For $Ni_{0.60}Mn_{2.40-x}In_xO_4$ the phase transition is at $x=0.75$ above which the cubic spinel phase is stable. Indium additions of more than 1.32 lead to secondary phases like In_2O_3 and NiO. For $x=0$ (no indium) samples contain additional NiO and are no longer single phase, according to Fig. 3, thus have not been considered in lattice calculations.

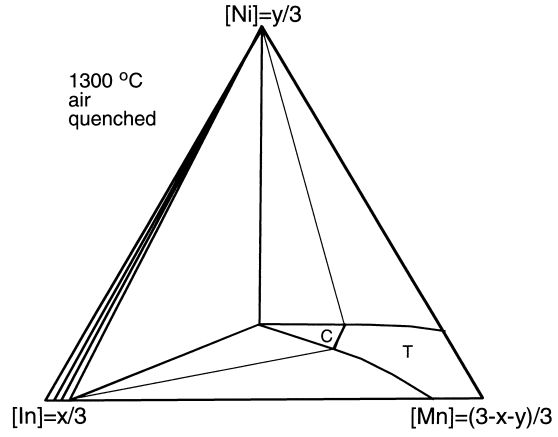

Fig. 3. The first-order approximated oxide phase diagram of Mn–Ni–In quenched in air from 1300°C (normalized metal concentrations according to $Mn_{3-x-y}In_xNi_yO_4$). C and T denote cubic and tetragonal phase fields, respectively.

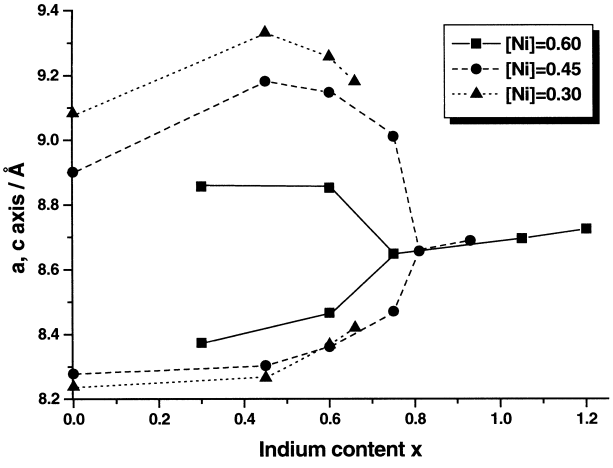

Fig. 4. The unit cell parameters a, c as a function of the indium content x for the three solid solutions according to the formula $Mn_{3-x-y}In_xNi_yO_4$ (pseudo-cubic face-centred cell with $c>a$).

For [Ni] = 0.45 the single spinel phase could be observed up to 0.96 In (see Fig. 5 as an example for secondary electron imaging in the SEM). Further amounts of In revealed secondary phases of Mn-doped In_2O_3 with cubic bixbyite structure. For [Ni] = 0.30 same behaviour of the lattice constants a, c in the tetragonal spinel phase range was found: the value of the c-axis increases up to $x = 0.45$ and decreases thereafter. In contrast to compounds with [Ni] = 0.45, there is no transition point to a cubic spinel phase, because for $x > 0.66$ the cubic bixbyite structure of In_2O_3 could be observed.

If the results of Fig. 4 are compared with each other, it can be seen that the transition from tetragonal to cubic spinel phase is observed for the different composition formulas at nearly the same indium content, i.e. at an x of about 0.77, excluding the samples with a Ni content of 0.3 for which an extrapolation appears to be rather hazardous because the samples become multiphase for $x > 0.67$. It is well known that the tetragonal-to-cubic phase transition in manganites occurs if the Mn^{3+} concentration on the octahedral sites becomes lower than 60%.[11] At higher values the octahedra along the c axis align cooperatively which leads to the tetragonal distortion. This means that at this point the $Mn^{(3+)}$ concentration on the octahedral sites is at least 60% and that the other 40% of the cations on these sites are from the Ni^{2+} and In^{3+} ions. To have 40% cations on the octahedral sites for different nickel contents, the indium ions have to fill up the sites to the desired amount of the cations. If the general accepted assumption of all Ni^{2+} ($y_{max} = 0.6$) and $Mn^{3+/4+}$ (60% of B-sites $= 1.2$) on octahedral sites is valid, there would have to be expected a transition point at an indium concentration of $x = 0.2$ which is definitely not observed in the experiments. As a consequence one can conclude that In has an first-order approximated tendency to the A-sites, but occupation of the octahedral lattice sites seems to increase with increasing In content, too. This situation appears to be comparable to that in the studies of Battault et al. with respect to the Fe occupation in the iron manganite spinels.[13] Further theoretical calculations which were performed by varying occupancy values for the different cations and for octahedral and tetrahedral sites lead to the conclusion that there is no single site preference for all ions and the situation appears to be comparable with the Fe system[9] but even more complicated. From the experimental data it is not possible to determine the exact proportion of In ions on the specific sites.

It has to be noticed again that all samples have been quenched from the sintering temperature of 1300°C and thus they are not in a thermodynamic equilibrium state. As a consequence this could produce behaviours and cationic distributions from which appropriate models are even more difficult to derive.

3.4. Electrical measurements

In order to investigate the range in specific resistivities and thermal constants which can be obtained for spinels in the system Mn–Ni–In–O, the ceramic samples of the

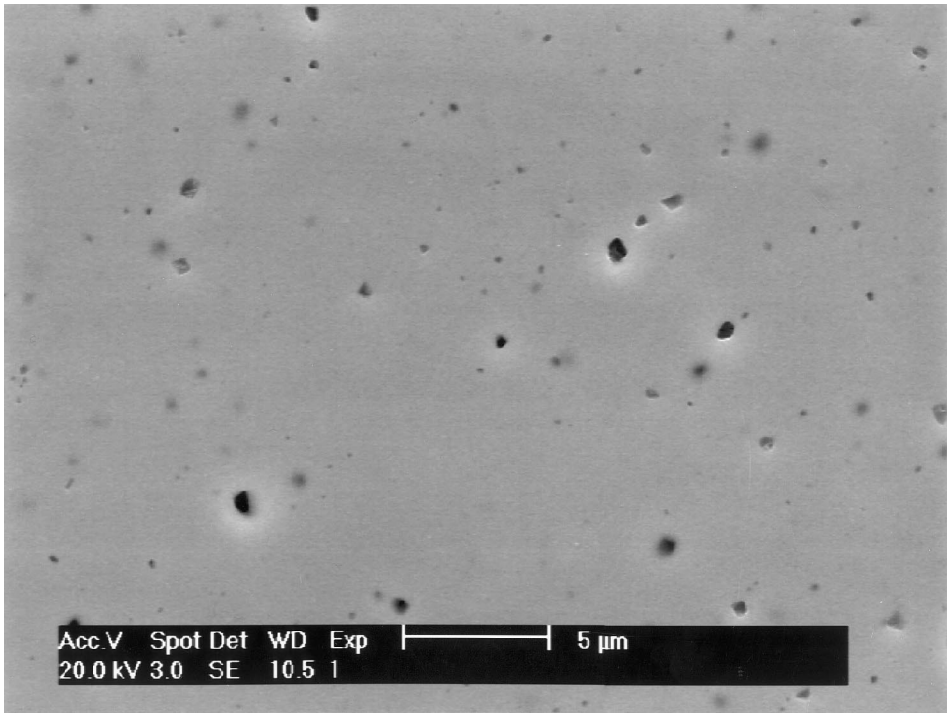

Fig. 5. Microstructure of the compound $Mn_{2.25}In_{0.3}Ni_{0.45}O_4$ investigated by SEM.

series given in the previous section were electrically measured. The average resistance of 16 ceramic pellets for each composition was determined at 25 and at 85°C and the averaged $B_{25/85}$ value for each composition was calculated. The values of the specific resistivity and the thermal constant as a function of the indium content for the three solid solutions were determined and the results are plotted in Figs. 6 and 7, respectively.

The results show clearly the dependence of the electrical values on the composition values. Fig. 6 reveals that the increase of the resistivity is dependent on the content of indium in the ceramics. The relative change of the resistivities between the three curves with various nickel contents ($y=0.30$, $y=0.45$ and $y=0.60$) is due to the different ratios between the Mn^{4+} and Mn^{3+} concentration or the carrier concentration. Remarkable is the increase of the resistivity for samples with a constant nickel content of 0.45 and 0.60: the logarithmic resistivity is a relatively linear function of the indium content. As already stated in the introduction it is well known that the addition of nickel to Mn_3O_4 leads to the creation of a dynamic equilibrium of Mn^{4+}-Mn^{3+} and to positive holes as charge carriers for the hopping process. On the other hand we have a competing effect by the addition of indium, i.e. the incorporation of In leads to an increase in resistivity because In^{3+} as a substitute for Mn^{2+} on a tetrahedral site needs the restoration of Mn^{3+} from Mn^{4+} on octahedral sites. Therefore, one expects the resistivity to increase with increasing indium content.

For higher In concentrations than given in Fig. 6 the resistivity values are too large to be measured. Typical resistivity values for $Mn_{2.5}Ni_{0.5}O_4$ samples lie around 2 kΩcm, which is in agreement with our $Mn_{2.55}Ni_{0.45}O_4$ prepared here which shows a resistivity of $2.3\cdot10^4$ Ωmm as given in Fig. 6.

The results of the thermal constant ($B_{25/85}$) are presented in Fig. 7. It is shown that the thermal constant increases linearly for the curve with $y=0.60$. For $y=0.45$ there seems to be a saturation of $B_{25/85}$ at 5100 from an In concentration of 0.75 on. The $B_{25/85}$ values show a large increase if the indium content is larger than $x=1.05$ and the same behaviour was observed for [Ni] = 0.30 if the addition of indium is larger than 0.3. Although it is obvious that an increasing B value corresponds to a more hindered hopping conduction process, it is still unclear why the two curves for [Ni] = 0.45 and 0.60 show different sign in second derivative with increasing indium content and more data has to be gained from further experiments.

4. Summary and conclusions

The phase diagram of Mn–Ni–In-O at 1300°C of quenched samples was determined in some important parts. The addition of In leads to the formation of single phase NTCs of the well known spinel structure. On the Mn rich side of the system samples revealed a tetragonal structure, whereas on the In rich side the single phase samples have the cubic spinel structure. In three series with fixed Ni amounts of 0.30, 0.45 and 0.60 the cubic-to-tetragonal phase transition takes place at the same In content of about 0.77. Only some minor secondary phases like In_2O_3 and NiO were found in samples with [Ni] = 0.60 by SEM not detected by XRD if the total In concentration exceeds 1.32. A linear increase of the thermal constant and logarithmic resistivity for samples with a nickel content of 0.45 and 0.60 as a function of the indium content have been observed. Together with the results for the lattice parameters as a function of In content, one can conclude that In^{3+} is partially divided among the tetrahedral and octahedral sites. Although Ni^{2+} and Mn^{3+} have a very strong preference for the octahedral site[12] and are still located there to care for the conductivity of the material, some substitution has to take place in order to alter the Mn^{3+}/Mn^{4+} ratio and hence explain for the decrease in resistivity with increasing Ni content.

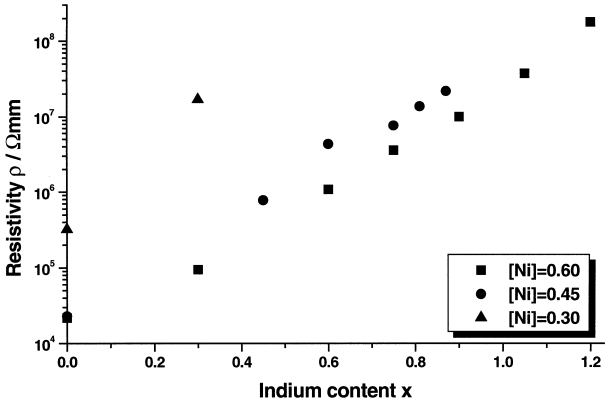

Fig. 6. The specific resistivity ρ as a function of the indium content x for the three solid solutions according to the formula $Mn_{3-x-y}In_xNi_yO_4$.

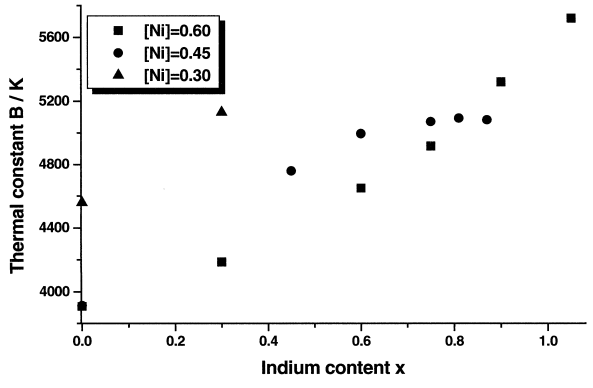

Fig. 7. The thermal constant $B_{25/85}$ as a function of the indium content x for the three solid solutions according to the formula $Mn_{3-x-y}In_xNi_yO_4$.

In this work the microstructural characterization has been performed on the as-sintered samples, but the electrical properties as a function of time (aging phenomena) are of special interest. They are under current investigations together with more thorough microstructural investigations by SEM and transmission electron microscopy and will be presented in a forthcoming report.

Acknowledgements

The authors would like to thank the assistance of P. Huppertz, K. Herff, J. Merx for preparation and light microscopical studies, H.D. Bausen for great support in X-ray diffraction analysis and the referee for stimulating discussion and review of the article.

References

1. Rousset, A., Legros, R., Caffin, J. P. and Lagrange, A., Low electrical resistivity NTC thermistors with long term stability, In *2nd Int. Conf. Passive Components: Materials, Technologies, Processing*. 1987, pp.97–102.
2. Hata, T., Kuroda, T. and Matsuo, Y., New thermistor materials. *Nat. Tech. Rep. (Japan)*, 1982, **28**, 1123–1134.
3. Battault, T., Legros, R., Brieu, M., Couderc, J. J., Bernard, L. and Rousset, A., Correlation between microstructure and ageing of iron manganite thermistors. *J. Phys. III France*, 1997, **7**, 979–992.
4. Sarrion, M. L. and Morales, M., Preparation and characterization of NTC thermistors: nickel manganites doped with lithium. *J. Am. Cer. Soc.*, 1995, **78**, 915–921.
5. Töpfer, J., Feltz, A., Dorbor, P. and Doumerc, J. P., Thermopower analysis of substituted nickel manganite spinels. *Mat. Res. Bull.*, 1994, **3**, 225–232.
6. Feltz, A. and Neidnicht, B., Investigations on electronically conducting oxide systems XX. $MgNiMnO_4$ and properties of $Mn_zNiMn_{2-z}O_4$ spinels. *J. All. Comp.*, 1991, **177**, 149–158.
7. Feltz, A. and Seidel, A., Untersuchungen an elektronenleitenden Oxidsystemen. XXI Stabile Spinelle $Zn_zNiMn_{2-z}O_4$ und Vergleich mit Spinellen $Mg_zNiMn_{2-z}O_4$. *Z. Anorg. Allg. Chem.*, 1992, **608**, 166–172.
8. Castelan, P., Ai, B., Loubiere, A., Rousset, A. and Legros, A., Aging study of nickel-copper manganite negative temperature coefficient thermistors by thermopower measurements. *J. Appl. Phys.*, 1992, **72**, 4705–4709.
9. Battault, T., Legros, R. and Rousset, A., Electroceramics made of iron-nickel manganite spinels: synthesis and microstructural and electrical properties. *J. Mat. Syn. Proc.*, 1996, **4**, 361–370.
10. Larson, E. G., Arnott, R. J. and Wickham, D. G., Preparation, semiconduction and low-temperature magnetization of the system $Ni_{1-x}Mn_{2+x}O_4$. *J. Phys. Chem. Solids*, 1962, **23**, 1771–1781.
11. Wickham, D. G., Solid-phase equilibria in the system NiO-Mn_2O_3-O_2. *J. Inorg. Nucl. Chem.*, 1964, **26**, 1369–1377.
12. Krupicka, S. and Nowak, P., *Ferromagnetic Materials* (Vol. 3), North-Holland Publishing Company, Amsterdam, 1982, p. 211.
13. Battault, T., Legros, R. and Rousset, A., Structural and electrical properties of iron manganite spinels in relation with cationic distribution. *J. Eur. Ceram. Soc.*, 1995, **15**, 1141–1147.